A High Resolution High Kinetic Energy Ion Mobility Spectrometer Based on a Low-Discrimination Tri-State Ion Shutter

Ansgar Thomas Kirk, Denise Grube, Tim Kobelt, Cornelius Wendt, and Stefan Zimmermann

Anal. Chem., **Just Accepted Manuscript** • DOI: 10.1021/acs.analchem.7b04586 • Publication Date (Web): 06 Apr 2018

A High Resolution High Kinetic Energy Ion Mobility Spectrometer Based on a Low-Discrimination Tri-State Ion Shutter

Ansgar T. Kirk*, Denise Grube, Tim Kobelt, Cornelius Wendt, Stefan Zimmermann

Leibniz Universität Hannover, Institute of Electrical Engineering and Measurement Technology, Department of Sensors and Measurement Technology, Appelstr. 9A, 30167 Hannover, Germany

*email: kirk@geml.uni-hannover.de

Abstract

High Kinetic Energy Ion Mobility Spectrometry (HiKE-IMS) allows for sensitive trace gas analysis within seconds, mitigating many disadvantages of standard ion mobility spectrometers through operation at reduced pressure and high electric field strengths. However, these advantages usually come at the cost of reduced resolving power, ranging from a maximum of 75 down to 50 at a reduced field strength of 120 Td for the original device. In this work, we present an extended theory for HiKE-IMS resolving power and a novel tri-state ion shutter principle able to achieve initial ion packet widths of 1 µs without significant mobility discrimination. Such an ultra-short injection time allows for improving the resolving power of the HiKE-IMS to 140 for a wide range of reduced electric field strengths. With this resolving power, separating all ion species generated from a mixture of benzene, toluene and xylene is possible. Furthermore, a resolving power of 140 is sufficient to partially separate isotopologues under high electric field strengths.

Introduction

Ion mobility spectrometers (IMS) characterize and separate ions by their motion through a neutral gas under the influence of an electric field [1]. Especially, this separation capability allows using atmospheric pressure chemical ionization (APCI) sources, which require differentiation between reactant ions and the various product ions formed. Due to their extremely high ionization efficiency for proton and electron affine compounds, APCI-IMS can achieve limits of detection in the low ppt_v-range for measurement times of less than a second [2].

One of the key parameters affecting ion motion and other gas phase ion processes is the reduced electric field strength *E/N*, the ratio of electric field strength *E* to neutral molecule density *N*, usually given in Townsend (Td) [3]. The drift velocity v_d strongly depends on the E/N value not only at high electric field strengths, where the alpha function needs to be considered, but also at low electric field strengths when expressed through the reduced ion mobility K_0 and the neutral density at standard conditions N_0, which is the Loschmidt constant, as shown by Eq. 1.

$$v_d = K_0 N_0 \frac{E}{N}\left(1 + \alpha_2\left(\frac{E}{N}\right)^2 + \cdots\right) \approx K_0 N_0 \frac{E}{N} \qquad (1)$$

The reduced electric field strength is a measure for the average energy gained between two collisions, as this energy can either be doubled by doubling the electric field strength or by doubling the average distance between two collisions. One analytical method that utilizes the dependence of gas phase ion processes on the reduced electric field strength is High Kinetic Energy Ion Mobility Spectrometry[4]. High Kinetic Energy Ion Mobility Spectrometers (HiKE-IMS) operate at reduced pressure and reduced electric

field strengths of up to 120 Td in the reaction region and the drift region. Using different reduced electric field strengths in the reaction region, it is possible to ionize compounds normally not ionizable through atmospheric pressure chemical ionization and to achieve a quantitative response to mixtures. These changes in reaction chemistry may be attributed to short-lived ions becoming detectable at much shorter residence times and to reactions and clustering being influenced by the vast increase in average ion energy. For example, benzene can be protonated and measured in the presence of toluene and xylene, despite the higher proton affinity and lower ionization energy of toluene and xylene[5]. Using different reduced electric field strengths in the drift region, it is possible to measure the ion mobility function K(E/N) over a wide E/N range instead of only K(0) as in low field ion mobility spectrometers or α(E/N) as in field asymmetric ion mobility spectrometers (FAIMS).

However, these HiKE-IMS strengths necessitate a two-fold improvement in resolving power. First, being able to ionize a broader spectrum of compounds means higher resolving power is needed to separate all the ionized compounds in a gas mixture. It is well-known that decreasing pressure decreases resolving power of an ion mobility spectrometer [6,7] and thus the current HiKE-IMS just achieves a resolving power of only 75 at its optimum drift voltage despite employing a drift cell that is able to reach a resolving power of 250 at atmospheric pressure [8]. Second, there is another, more subtle challenge when it comes to the resolving power of HiKE-IMS. Every drift tube ion mobility spectrometer has an optimum drift voltage which maximizes its resolving power. Usually, it is operated at this value or slightly above to achieve improved limits of detection [9]. However, in HiKE-IMS, the drift voltage is no longer an independent variable that can be set to maximize resolving power, since it is now defined by the desired reduced electric field strengths. Thus, HiKE-IMS does not simply need improved resolving power at a fixed drift voltage, but improved resolving power across the whole range of desired reduced electric field strengths. As these requirements differ from those of atmospheric pressure IMS, existing theory is not fully applicable and thus needs to be extended in order to include these constraints and to identify which instrumental parameters possess the largest influence on resolving power.

Theoretical Model

In order to understand the resulting challenges and especially the relationships between parameters, an analytical model is a useful tool. The resolving power of an ion mobility spectrometer is defined as the ratio between the drift time t_d and the full width at half maximum $w_{0,5}$ and can be estimated by eq. 2 [10,11,2].

$$R_p = \frac{t_D}{w_{0,5}} = \frac{\frac{L^2}{K\,U_d}}{\sqrt{{w_{min}}^2 + \frac{16\,\mathrm{k_B}\,T\ln 2}{z\,\mathrm{e}\,U_d}\left(\frac{L^2}{K\,U_d}\right)^2}} \qquad (2)$$

Its parameters are the drift length L, the drift voltage U_d, the minimum peak width w_{min} accounting for initial ion packet width and amplifier distortion, the ions' mobility K and their charge state z as well as the absolute temperature T.

However, for analyzing the resolving power in HiKE-IMS, it is more adequate to rewrite eq. 2 as a function of the reduced electric field strength rather than drift voltage, leading to eq. 3 with ε representing the reduced electric field strength, $\varepsilon = E/N$.

$$R_p = \frac{\frac{L}{K\,N\,\varepsilon}}{\sqrt{{w_{min}}^2 + \frac{16\,\mathrm{k_B}\,T\,\ln 2}{z\,\mathrm{e}\,L\,N\,\varepsilon}\left(\frac{L}{K\,N\,\varepsilon}\right)^2}} \quad (3)$$

In practical designs, two of the terms are implicitly dependent on the neutral density *N*. This must be considered in order to obtain a useful model. First, the ion mobility K depends on the neutral gas density N and should thus be replaced by the reduced mobility given by eq. 4, which is the mobility under standard conditions. Second, as the required drift voltage in HiKE-IMS can easily become several ten kilovolts, the maximum available drift voltage U_{max} also becomes a limiting factor that is related to drift length L, neutral gas density N and maximum desired reduced electric field strength ε_{max}. Longer drift tubes require lower pressures in order to be able to reach the same reduced electric field strength at the same available voltage, a relationship given through eq. 5. It should be noted that these substitutions are also correct for other ion mobility spectrometers if operation at a specific reduced electric field strength is required.

$$K = \frac{K_0\,N_0}{N} \quad (4)$$

$$U_{max} = \varepsilon_{max}\,N\,L \quad (5)$$

Inserting these two relationships into eq. 3 and diving it by the numerator yields eq. 6.

$$R_p = \frac{1}{\sqrt{\left(K_0\,N_0\,\frac{w_{min}}{L}\,\varepsilon\right)^2 + \frac{16\,\mathrm{k_B}\,T\,\ln 2}{z\,\mathrm{e}}\,\frac{\varepsilon_{max}}{U_{max}}\,\frac{1}{\varepsilon}}} \quad (6)$$

The first term in the denominator still represents the maximum achievable resolving power limited by the minimum width accounting for initial ion packet width and amplifier distortion, while the second term still represents the maximum achievable resolving power limited by diffusion. The first term can be varied by varying the ratio of minimum width w_{min} to drift length *L*. At the same reduced electric field strength, the drift velocity is always the same according to Eq. 1. Thus, doubling the drift length will double the drift time, while halving the minimum width w_{min} will halve the width of the measured peak when diffusion becomes negligible. Both approaches thus result in doubling the resolving power at very high reduced electric field strengths. According to eq. 5, doubling the drift length also means halving the pressure, even though the pressure or neutral density does not explicitly appear in eq. 6. The neutral density has to change because it was the variable eliminated from eq. 6. However, significantly increasing the drift length is not a feasible approach, as it leads to a rather large device. Furthermore, the resolving power only scales linearly with drift length under HiKE-IMS conditions, while it scales with the square of the drift length for ion mobility spectrometers operated at their optimum drift voltage. However, the resolving power scales linearly with the inverse of the minimum width in both cases. Thus, reducing the minimum width is the most viable option for significant resolving power improvements in HiKE-IMS.

The second term can be varied by varying the ratio of the highest desired reduced electric field strength to the maximum available voltage. Lowering the maximum reduced electric field strength would mean giving up HiKE-IMS conditions, and thus, the only way for improvement is increasing the maximum drift voltage available. Again, due to Eq. 5, doubling the maximum drift voltage also means doubling the pressure. It should be noted that increasing the drift voltage not only requires larger high voltage power supplies, but also better shielding of critical components to prevent arcing. While specialized norms such as the IEC-60950 provide detailed information, observing general rules often suffices. Typically, electrical breakdown will either occur through a gap, estimated at 3 kV/mm in dry air at atmospheric pressure, or across a surface, estimated at 1 kV/mm across a clean surface regardless of pressure. Thus, for high potential differences outside the vacuum, e.g. between corona or shutter electronics and a grounded case, not only sufficient gap distances or insulation thicknesses are required, but also the mounting flange must offer a sufficient creepage distance across its surface. For high potential differences inside the vacuum, e.g. between corona needle and a grounded membrane pump, only the gap distances need to be observed, but must be sufficiently increased to account for the reduced pressure, as the breakdown voltage of large gaps decreases according to Paschen's law. However, reducing the pressure always increases the breakdown reduced electric field strength. Thus, as a breakdown of 3 kV/mm at atmospheric pressure already equals 120 Td, at a pressure of only 20 mbar no special precautions should be necessary to achieve a reduced electric field strength of 120 Td in a drift tube. In fact, we are using our standard atmospheric pressure drift tube[8] without any modifications.

Analogous to previous models [2], the optimum reduced electric field strength and the optimum resolving power under these conditions can be calculated as given by Eq. 7 and 8.

$$\varepsilon_{opt} = \sqrt[3]{\frac{8\,\mathrm{k_B}\,T\,\ln 2}{{K_0}^2\,{N_0}^2\,z\,\mathrm{e}}\,\frac{\varepsilon_{max}}{U_{max}}\,\frac{L^2}{{w_{min}}^2}} \qquad (7)$$

$$R_{opt} = \sqrt[3]{\frac{z\,\mathrm{e}}{24\,K_0\,N_0\,\mathrm{k_B}\,T\,\ln 2}\,\frac{U_{max}}{\varepsilon_{max}}\,\frac{L}{w_{min}}} \qquad (8)$$

In HiKE-IMS, Eq. 7 and 8 are not as important as for ion mobility spectrometers operated at their optimum resolving power, but they nevertheless reveal several interesting relationships. All three options for improving the resolving power will yield the same increase of resolving power at the optimum reduced electric field strength. However, while increasing the length or decreasing the minimum width increases the higher optimum reduced electric field strengths, increasing the maximum available drift voltage decreases the optimum reduced electric field strength. Thus, for better resolving power across a wide range of reduced electric field strengths, a combination of the two approaches is advisable as shown in Figure 1.

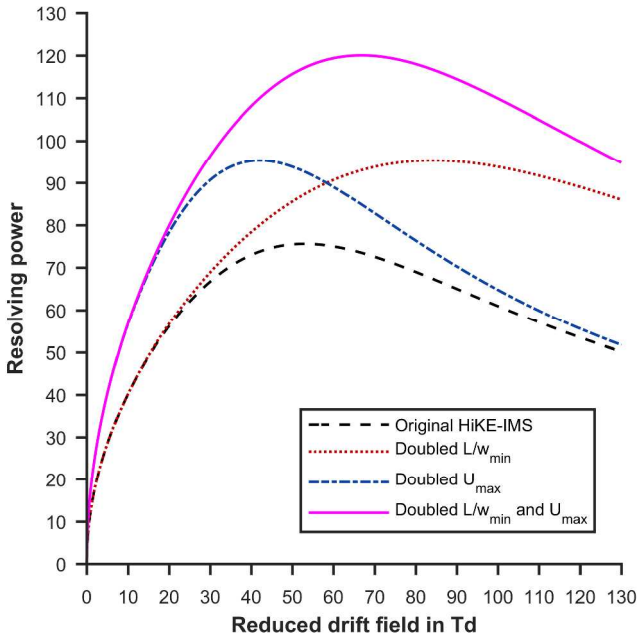

Figure 1: Theoretical resolving power over applied reduced electric field strength for the first HiKE-IMS (dashed black line), for doubled ratio of length L to minimum width w_{min} (dash-dotted blue line), for doubled maximum drift voltage U_{max} (dotted red line) and for both doubled L/w_{min} and doubled U_{max} (solid magenta line).

Tri-state ion shutter method

As the previous HiKE-IMS was already operated at initial ion packet widths in the low microsecond range [5], a significant reduction requires an ion shutter capable of achieving single microsecond initial ion packet widths. As discussed before [12], an ion shutter capable of reaching low initial ion packet widths requires low field distortion in the drift region and a low cutting width. First, field distortion can both be caused by changing potentials on electrodes directly neighboring the drift or reaction region or by several potentials existing in a single plane, which lead to electrical fields orthogonal to the drift direction. It causes tailing and ion accumulation / depletion effects through ions being caught in low field strength regions[13,14] Second, as an ion shutter has to inhibit ion motion in the closed state, it necessarily creates a region in which ions cannot exist. When the shutter is opened, ions start traversing this elimination region from its beginning, but only the ions having fully passed it are actually injected before the shutter closes again. All other ions are eliminated upon closing, cutting off the rear portion of the ion packet at the end of the elimination region. Therefore, the initial ion packet width will be shorter than the applied electrical injection pulse width by the time the ions need to traverse the elimination region, which is called the cutting width[15]. When a suitable injection pulse width for fast ions is chosen, slow ions will be missing from the spectrum and when a suitable injection pulse width for slow ions is chosen, fast ion will exhibit broad peaks.

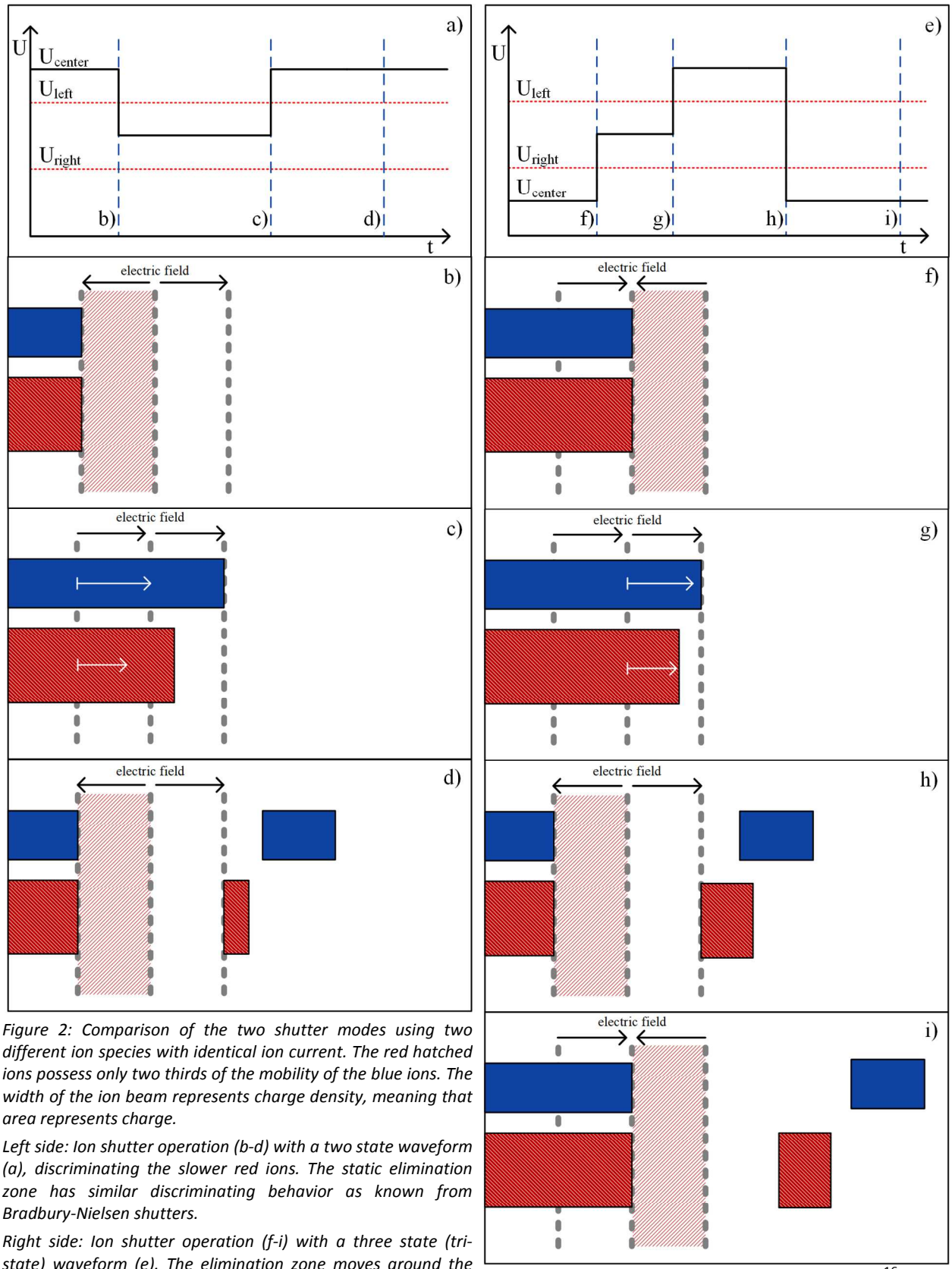

Figure 2: Comparison of the two shutter modes using two different ion species with identical ion current. The red hatched ions possess only two thirds of the mobility of the blue ions. The width of the ion beam represents charge density, meaning that area represents charge.

Left side: Ion shutter operation (b-d) with a two state waveform (a), discriminating the slower red ions. The static elimination zone has similar discriminating behavior as known from Bradbury-Nielsen shutters.

Right side: Ion shutter operation (f-i) with a three state (tri-state) waveform (e). The elimination zone moves around the ion packet, thus preventing discrimination.

The well-known Bradbury-Nielsen shutter [16], used in most IMS, suffers severely from these two non-

idealities [17,15,12–14] and therefore its typical injection pulse widths are 50 µs or larger [18–21,6,11]. The Tyndall-Powell shutter [22] does usually possess an even larger cutting width due to the spacing between its two electrodes, however, an improved operating mode allows reducing the injection pulse width to 40 µs without inducing significant ion discrimination[23].

In order to reach significantly smaller initial ion packet widths, we use a so-called field switching shutter[24,25,12] for our high resolution IMS [8], which has zero cutting width and no field inhomogeneities[12]. This way, initial ion packet widths as low as 5 µs are achievable without measurably discriminating slower ions[12]. Unfortunately, the field switching shutter requires ionization in a field-free region and is thus not applicable to many ion sources, including the HiKE reaction region. Approaches to integrate field switching with other shutter methods are known [26,27], but so far none of these approaches could reach the single-microsecond initial ion packet widths of a field switching shutter.

Together with the previous HiKE-IMS, a simple three grid shutter was introduced [5]. In the closed state, the center grid is switched to a higher potential, blocking the passage of ions. In the open state, its potential is lowered as shown in panel a) of Figure 2, creating a constant potential gradient across shutter and drift region. This is free from field inhomogeneities and mechanically simple to construct, but the cutting width is equal to the distance between two grids. Both the cutting width and the resulting discrimination are shown in panel b) to d) of Figure 2. The two ion beams have identical ion currents, but the mobility of the red hatched ions is only two thirds of the mobility of the blue ions. Therefore, to fulfill the assumption of identical ion currents, the red ion beam must possess fifty percent more ion density than the blue ion beam, which is illustrated through the fifty percent larger width. This way, area represents charge and a direct visual assessment of discrimination is possible. The moment the ion shutter is opened, both ion beams start to traverse the elimination region as shown in panel b), covering a distance proportional to their mobility as shown in panel c). At this point, the shutter is closed again, but only the part of the ion packet behind the elimination region is actually injected. While in panel c) the same amount of ions had passed the first grid after opening, the amount actually injected is vastly different as shown in panel d). Thus, none of the currently used ion shutter principles fulfill the requirement of creating single microsecond initial ion packet widths from the ions leaving the reaction region of the HiKE-IMS.

This disadvantage can be overcome by using a three grid shutter in combination with two closed states in a specific sequence [28] shown in panel e). As it possesses three different switching states, we call this the tri-state ion shutter. When a potential higher than the potential of the first grid is applied to the center grid, the left side of the shutter is closed. When a potential lower than the potential of the third grid is applied to the center grid, the right side of the shutter is closed. As shown in panel f) to i) of Figure 2, it is possible to combine these two closed states in order to mitigate ion discrimination. First, the lower potential is applied to the center grid, closing the right shutter region. Ions are now moving from the reaction region up to the center grid as shown in panel f). To open the shutter, a potential restoring the potential gradient across the drift tube is applied. The ions now enter the drift region, starting their movement from the center grid as shown in panel g). To close the ion shutter, the higher potential is applied to the center grid, closing the left region and pushing the ions from the right shutter region into the drift tube as shown in panel h). The ions in the left side are discharged. However, since the ion packet started moving from the center grid and is cut off at the center grid, no ion discrimination occurs and the injected amount of ions is the same for both ion species. The elimination zones still exist, but they are now moved around the ion packet during injection. After all ions have left the shutter, the

lowest potential is applied to the center grid again as shown in panel i). When switching back from high to low potential, the cutting width is effectively doubled, preventing an unwanted second ion injection.

Videos of COMSOL simulations illustrating the difference between the two shutter modes can be found in the supporting information. It should be noted that the simulations were carried out in 2D to keep reasonable computational costs and therefore overestimate effects in the center of the shutter grid holes.

Experimental

The measurement setup used in this work is similar to the previous HiKE-IMS reported by our lab [4,5]. The vacuum system has remained the same, using a MVP-040 membrane pump (Pfeiffer Vacuum) with an EVN-116 gas dosing valve (Pfeiffer Vacuum) for evacuation and a CMR-362 capacitive pressure gauge (Pfeiffer Vacuum) for pressure monitoring. Drift gas is supplied using an F-200DV-ABD mass flow controller (Bronkhorst). Sample gas is transferred into the HiKE-IMS via a 750 µm inner diameter capillary, whose length has been adjusted to provide the desired sample flow rate. Purified air or purified nitrogen was used as both drift and sample carrier gas. All chemicals used in this work were purchased from Sigma-Aldrich Germany with a purity > 99 % and introduced into the gas mixing system via a Vici Dynacalibrator Model 150 permeation oven and home-made permeation tubes. A controllable fraction the gas flow from the permeation oven is further diluted with clean gas to obtain the desired analyte concentration. As only two permeation ovens are present per gas mixing systems, mixtures containing more than two compounds must be created by introducing more than one analyte through a single oven.

However, several modifications and improvements have been made to the electrical setup in order to accommodate the tri-state ion shutter. In this work, the operating pressure was to be maintained at 20 mbar in order to prevent unwanted changes in reaction chemistry which are outside of the current works scope. The original drift tube has been replaced by two conjoined drift tubes based on the design used before [8], forming a 306 mm long drift region. Furthermore, the electronics have been modified to reach higher drift voltages, which are now supplied by a 20 kV power supply from FuG. In combination, the longer drift tube and the higher drift voltage allow maintaining the operating pressure at 20 mbar as explained by Eq. 5. All other voltage sources and voltage switches used to control the ion shutter, reaction region and corona were developed and built at our lab. They are isolated by 35 kV with respect to ground. Especially, a new shutter controller board was developed, which is able to generate the three potential waveform needed to operate the shutter. All four necessary voltages (two between the grids, two for the positive and negative pulse) can be set individually and the pulse has a rise time of only 15 ns and a timing resolution of 10 ns. The voltages are linked to the reduced field strength value set for the drift region in order to always maintain the waveforms shown in panels a) and e) of Figure 2. To implement the switching between three potentials, two MOSFET half bridges are used in series. As the largest isolated power supply available to us at the moment is limited to 5 kV, the reaction region had to be shortened from 108 mm to 77 mm in order to maintain the same possible reduced field strength range. The corona discharge ion source has remained unchanged from the original setup.

Furthermore, instead of the custom-built transimpedance amplifier used in the second publication [5,29], a commercial DLPCA-200 (Femto) transimpedance amplifier was used as in the first work [4], as its bandwidth can be selected in several steps. It was set to 400 kHz, yielding a rise time of about 1 µs in order to match the shorter injection widths as required [2]. Measurement data were digitized using an U1082A digitizer with on-board averaging (Keysight) using an acquisition time of five seconds per

spectrum. As its lowest possible analog bandwidth setting is 20 MHz, data were filtered afterwards to reduce the bandwidth again to that of the ion mobility spectrum. The new operational parameters are summarized in Table 1.

Table 1: Operational parameters of the new high resolution HiKE-IMS setup

Parameter	Value
Reaction region length	77 mm
Drift region length	306 mm
Drift region diameter	21 mm
Corona voltage	1200 V
Reaction region voltage	Up to 5 kV
Reaction region reduced electric field	Up to 125 Td
Drift region voltage	Up to 20 kV
Drift region reduced electric field	Up to 125 Td
Injection time	Down to 1 µs
Repetition rate	200 Hz – 2 kHz
Drift gas flow	10 mls/min
Sample gas flow	10 mls/min
Dew point of drift gas and sample gas	-90 °C (90 ppb_v water vapor concentration)
Operating pressure	20 mbar
Operating temperature	25 °C

Results and discussion

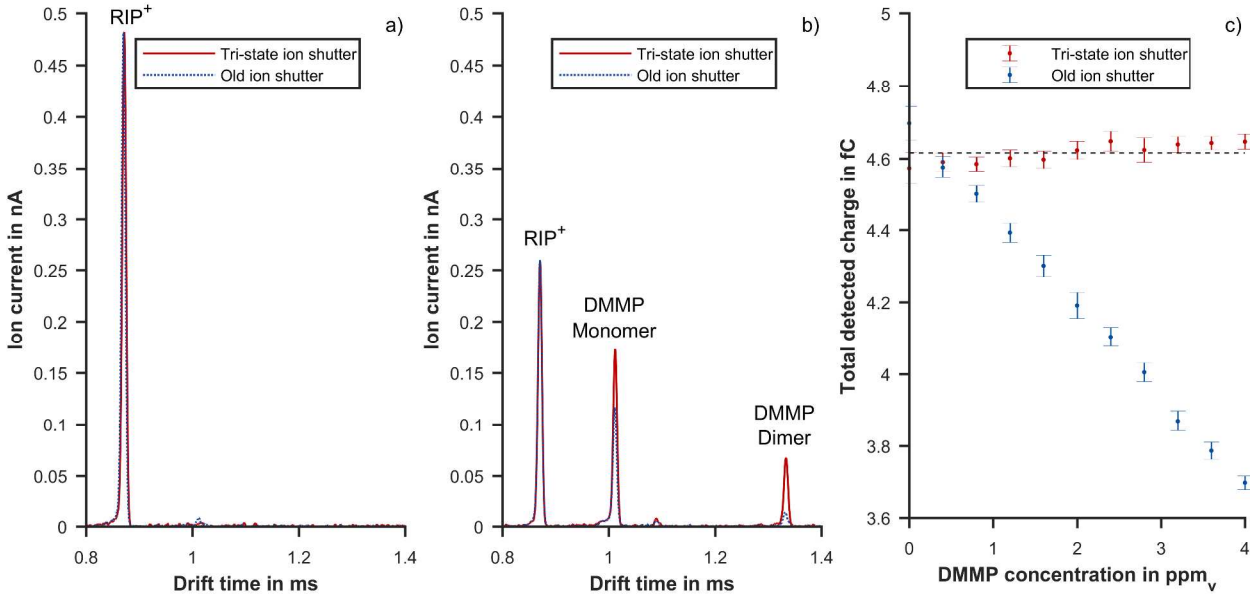

Figure 3: Spectra using the tri-state (red solid lines) and old (blue dotted lines) shutter mode when analyzing clean air (panel a)) and clean air with 4 ppm_v DMMP (panel b)) at reduced electric field strengths of 15 Td in the reaction and 60 Td in the drift region. The discrimination of slower ions at an identical reactant ion peak amplitude is clearly visible, which is also indicated by monitoring the total charge in the spectrum (panel c)). Error bars denote one standard deviation of the observed charge during a twenty minute interval of constant concentration.

The tri-state ion shutter mechanism and high resolution HiKE-IMS was first characterized using dimethyl methylphosphonate (DMMP). The injection pulse width of the tri-state ion shutter was set to 1 µs, while the injection pulse width of the old shutter was reduced from the original 6 µs to 3 µs, leading to identical reactant ion peaks as shown in panel a) of Figure 3. Since the same peak and thus the same initial ion packet width is achieved at an injection pulse width difference of 2 µs, the cutting width of the old shutter can be estimated at about 2 µs larger for the reactant ions.

As the next step, DMMP was added to the sample gas. It should be noted that an extremely high DMMP concentration in the ppm_v-range and a low reduced electric field strength of 15 Td in the reaction region is necessary to generate a significant dimer signal due to the high linear range of the HiKE-IMS. As shown in panel b) of Figure 3, the reactant ion peak decreases the same independently of the shutter mode. This indicates that the same amount of DMMP ions should have been formed in both modes, as the total charge generated by the corona discharge source should stay nearly constant. However, despite the same amount of generated DMMP ions, the amount of detected DMMP ions is significantly higher when using the tri-state ion shutter mode. About 50% more DMMP monomer ions and 400% more DMMP dimer ions arrive at the detector. While both shutter modes are able to produce a high resolution reactant ion peak, only the tri-state ion shutter allows for high product ion peak intensities at the same time. This reemphases the necessity of ion shutters with extremely low ion discrimination when operating at single microsecond initial ion packet widths.

To provide a further measure for the reduction in discrimination, the total detected charge in the spectrum is plotted in panel c) of Figure 3 against the concentration of DMMP in the sample gas. Increasing the DMMP concentration leads to the formation of slower ions, which experience a larger cutting width, leading to a decrease in the total charge observed at the detector. However, with the tri-state ion shutter mechanism, the total charge stays constant, indicating that this shutter does not discriminate the DMMP dimer ions compared to the reactant ions – at least no discrimination could be measured with the used setup. These observations also fit very well with a rough estimation of the expected discrimination mechanism. Assuming that the tri-state ion shutter is ideal, the reactant ion peak experiences a cutting width of about 2 µs during injection when using the old shutter, creating an initial ion packet width of 1 µs from an injection pulse width of 3 µs. Thus, the 15 % slower DMMP monomer will experience 15 % more cutting width, reducing its initial ion packet width to 0.7 µs at the same injection pulse width. This fits the intensity and thus initial ion packet width using the tri-state ion shutter well, which should correspond to the injection pulse width of 1 µs and is about 50 % higher.

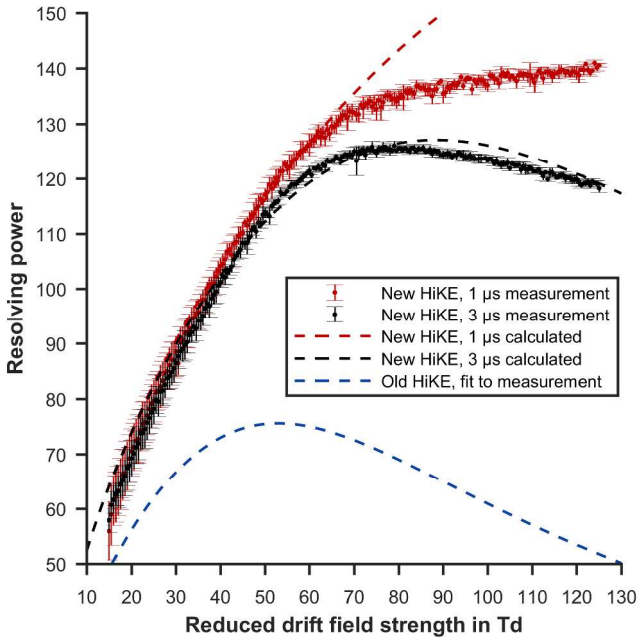

Figure 4: Measured resolving power for the peak of 0.9 ppm$_v$ methyl salicylate in the new high resolution HiKE-IMS using an initial ion packet width of 1 µs (red dots) and 3 µs (black dots). The resolving power was determined through a Gaussian fit. Error bars denote one standard deviation from five repetition measurements. Resolving power curves shown as dashed lines are all three calculated from the measured resolving powers of the previous HiKE-IMS [5]. Blue indicates the previous HiKE-IMS, black and red the new high resolution HiKE-IMS with the corresponding initial ion packet widths.

As a next step, the drift voltage was swept at two different initial ion packet widths, 1 µs and 3 µs. Methyl salicylate in clean air was used as sample gas. The resulting resolving powers are shown in Figure 4 together with resolving power curves calculated from the reported values of the previous HiKE-IMS. For an injection width of 3 µs, the resolving power curve calculated by scaling the measurement values of the previous HiKE-IMS based on eq. 6 fits the measurement values from the new high resolution HiKE-IMS well. For an initial ion packet width of 1 µs, however, the measured values nearly reach a plateau at reduced electric field strengths above 80 Td and thus diverge from the calculated curve. This might be caused by additional effects not included in eq. 6, such as the increase of the diffusion coefficient at higher ion energies due to higher reduced electric field strengths [3,30]. It is important to note that previously negligible non-idealities can rapidly gain influence due to the geometric addition in Eq. 6 when another term is reduced.

The maximum resolving power for an initial ion packet width of 1 µs is above R_p = 140, approximately twice the maximum resolving power of to the previous HiKE-IMS. At higher reduced electric field strengths, the gain in resolving power is even higher. However, the maximum resolving power would be reached outside the targeted reduced electric field strength range. Thus, using a slightly longer injection width, such as 3 µs, gives a better balance between resolving power and signal-to-noise ratio. Nevertheless, in future setups with shorter drift tubes at increased pressure, shorter initial ion packet widths than 3 µs are required to maintain high resolving power across a wide reduced electric field strength range.

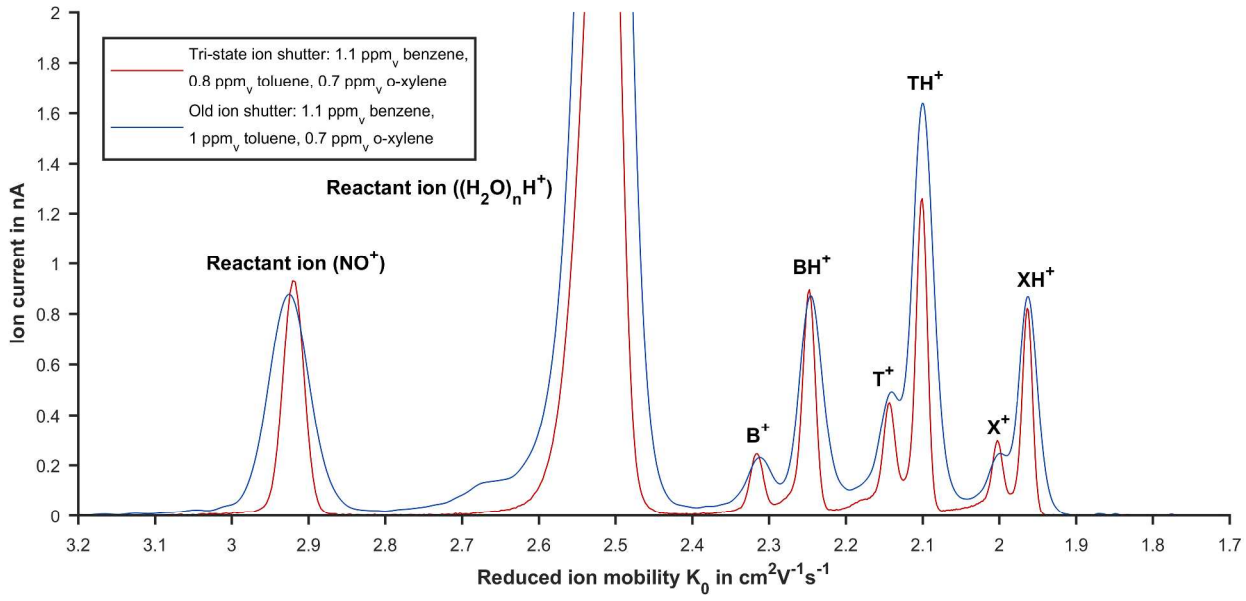

Figure 5: Measurement of a mixture of benzene, toluene and o-xylene (BTX) in clean air at a reduced field strength of 120 Td in the reaction and 90 Td in the drift region using the previous (blue) and the new high resolution (red) HiKE-IMS. The probable peak assignments were discussed in the original publication [5].

As a prominent example, the measurement of a mixture of benzene, toluene and o-xylene in clean air demonstrated in previous HiKE-IMS publications [5] was repeated using the new high resolution HiKE-IMS. As shown in Figure 5, the increased resolving power results in significantly improved peak separation. The peak pairs, corresponding to the directly ionized and the protonated molecule of the three substances, can be almost base-line separated with the new high resolution HiKE-IMS. Furthermore, due to the improved separation between the different substances, a raised baseline between the peaks can be revealed. These raised baselines contain additional information, as they can be caused by additional ion-molecule reactions, ion decomposition or fragmentation inside the drift tube[31–33]. This is especially important in HiKE-IMS, as its conditions allow the measurement of short-lived or otherwise non-existing ions. In Figure 5, especially the protonated product ion peaks show a strong fronting, which can in the case of toluene and o-xylene at least partially be attributed to their known fragmentation at high reduced electric field strengths[5]. However, this explanation does not hold for benzene. Thus, the most likely explanation appears to be a decomposition of the protonated product ions. It should be noted that the different peak intensities between former measurements from 2014 and measurements recorded in this work result from different self-made permeation tubes for producing a ternary mixture.

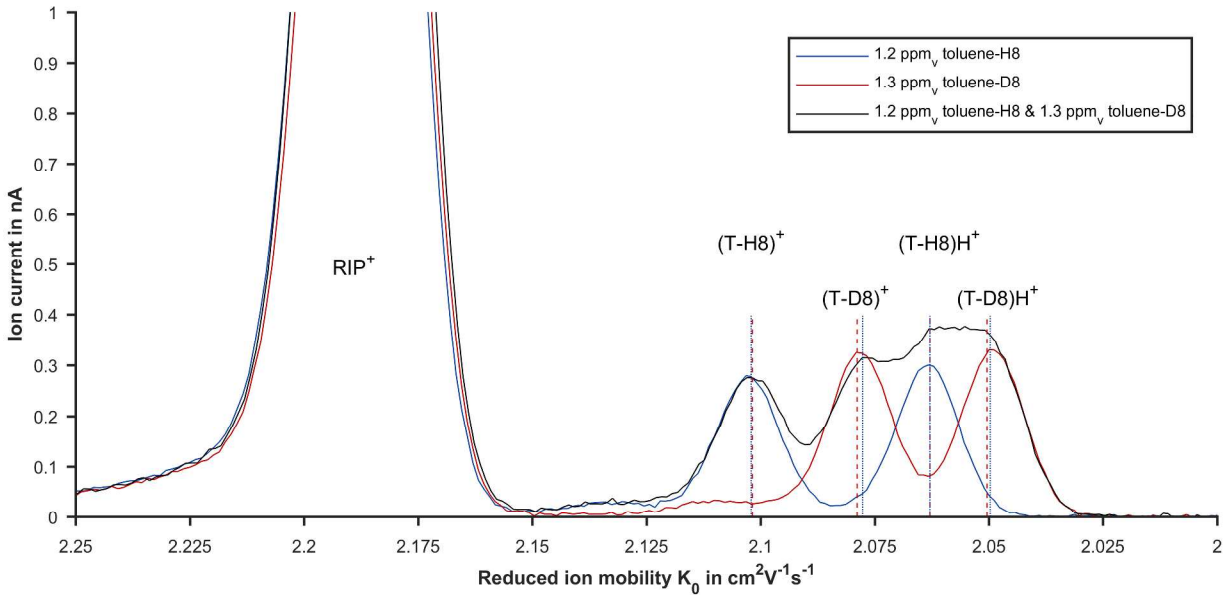

Figure 6: Measurements of toluene (blue), perdeuterated toluene (red) and a mixture (black) in nitrogen at a reduced field strength of 60 Td in the reaction at 60 Td in the drift region. Peak positions estimated from the mixture spectrum are indicated by red dashed lines for deconvolution and by blue dotted lines for Gaussian peak fitting.

Furthermore, we continued our previous studies of isotopologue separation by ultra-high resolution ion mobility spectrometry [34] with the new high resolution HiKE-IMS. This is of special interest, as the HiKE-IMS can provide additional reaction pathways and higher ion energies and thus new observations. Analyzing the mobility shift between isotopologues should not only provide information about limitations of the fundamental mobility equations, but may even allow the determination of ions masses[35]. Figure 6 depicts a measurement of regular and perdeuterated toluene. Each toluene peak is already a peak doublet as shown in Figure 5, due to direct ionization and protonation both being possible under HiKE-IMS conditions. Together with the mobility difference from the mass shift between the isotopologues, this results in a total of four overlapping peaks. Nevertheless, Gaussian peak fitting based on the known number of peaks or peak deconvolution[8] allow for estimating peak position from the mixture spectrum as shown in Figure 6. As the peak position is the only quantity required for determining the mobility shift, this is sufficient for isotopologue analysis under HiKE-IMS conditions. It is however important to keep in mind that an ion mobility spectrum contains much more information than mere peak position as already shown in Figure 5. Thus, improved resolving power will always be preferable to post-processing techniques which may be unable to recover important details.

Conclusion

In this paper, we presented a novel tri-state ion shutter mechanism allowing the construction of a HiKE-IMS with vastly improved resolving power across an increased range of reduced electric field strengths. The main advantage of the tri-state ion shutter is its extremely low mobility discrimination, which allows for the use of initial ion packet widths as low as 1 µs without losing intensity of slow ion species. This a significant improvement compared to existing ion shutter principles. The improvements of the ion shutter are augmented by a longer drift tube in this work to reach high resolving power of R_p = 140, but can also be used to construct compact HiKE-IMS with decent resolving power. For example, based on the presented measurement results, a HiKE-IMS with a 100 mm long drift region should still reach a resolving

power of about R_p = 120. Furthermore, the new high resolution HiKE-IMS enables additional separation of complex samples and even isotopologues, both of which are of high interest for future ion mobility studies. Additionally, the tri-state ion shutter mechanism is not limited to HiKE-IMS, but can be also applied to, for example, ion mobility spectrometers with atmospheric pressure corona sources, radioactive Nickel-63 sources or electrospray ionization sources. Especially the last application is very promising, as the reduced mobility discrimination is extremely important for larger ions from electrospray ionization sources. This will help the development of electrospray ionization ion mobility spectrometers with both high resolving power and low limits of detection.

Acknowledgments

Funded by the Deutsche Forschungsgemeinschaft (DFG, German Research Foundation) – ZI 1288/7-1.

ATK designed shutter concept, measurement setup and theoretical model. DG, TK and ATK performed most experiments and data analysis. CW designed the shutter control electronics. SZ supervised the research project, and gave scientific and conceptual advice. All authors contributed to discussions and the manuscript.

We thank Alexander Bohnhorst, André Ahrens, Arben Pulaj, Florian Schlottmann and Maria Allers for their help during this work.

References

(1) Eiceman, G. A.; Karpas, Z.; Hill, H. H. *Ion mobility spectrometry,* 3rd edn.; CRC Press: Boca Raton, 2013.
(2) Kirk, A. T.; Allers, M.; Cochems, P.; Langejuergen, J.; Zimmermann, S. *Analyst* **2013**, *138*, 5200–5207.
(3) Mason, E. A.; McDaniel, E. W. *Transport Properties of Ions in Gases*; Wiley-VCH Verlag GmbH & Co. KGaA: Weinheim, FRG, 1988.
(4) Langejuergen, J.; Allers, M.; Oermann, J.; Kirk, A. T.; Zimmermann, S. *Anal. Chem.* **2014**, *86*, 7023–7032.
(5) Langejuergen, J.; Allers, M.; Oermann, J.; Kirk, A. T.; Zimmermann, S. *Anal. Chem.* **2014**, *86*, 11841–11846.
(6) Tabrizchi, M.; Rouholahnejad, F. *Talanta* **2006**, *69*, 87–90.
(7) Davis, E. J.; Dwivedi, P.; Tam, M.; Siems, W. F.; Hill, H. H. *Anal. Chem.* **2009**, *81*, 3270–3275.
(8) Kirk, A. T.; Zimmermann, S. *Int. J. Ion Mobil. Spec.* **2015**, *18*, 17–22.
(9) Kirk, A. T.; Zimmermann, S. *Int. J. Ion Mobil. Spec.* **2015**, *18*, 129–135.
(10) Spangler, G. E.; Collins, C. I. *Anal. Chem.* **1975**, *47*, 403–407.
(11) Siems, W. F.; Wu, C.; Tarver, E. E.; Hill, Herbert H. Jr.; Larsen, P. R.; McMinn, D. G. *Anal. Chem.* **1994**, *66*, 4195–4201.
(12) Kirk, A. T.; Zimmermann, S. *Int. J. Ion Mobil. Spec.* **2014**, *17*, 131–137.
(13) Puton, J.; Knap, A.; Siodłowski, B. *Sens. Actuators, B* **2008**, *135*, 116–121.
(14) Du, Y.; Wang, W.; Li, H. *Anal. Chem.* **2012**, *84*, 1725–1731.
(15) Tabrizchi, M.; Shamlouei, H. R. *Int. J. Mass Spectrom.* **2010**, *291*, 67–72.
(16) Bradbury, N. E.; Nielsen, R. A. *Phys. Rev.* **1936**, *49*, 388–393.
(17) Tadjimukhamedov, F. K.; Puton, J.; Stone, J. A.; Eiceman, G. A. *Rev. Sci. Instrum.* **2009**, *80*, 103103.
(18) Rokushika, S.; Hatano, H.; Baim, M. A.; Hill, H. H. *Anal. Chem.* **1985**, *57*, 1902–1907.
(19) Eiceman, G. A.; Nazarov, E. G.; Rodriguez, J. E.; Stone, J. A. *Rev. Sci. Instrum.* **2001**, *72*, 3610–3621.

(20) Kanu, A. B.; Gribb, M. M.; Hill, H. H. *Anal. Chem.* **2008**, *80*, 6610–6619.
(21) Spangler, G. E. *Int. J. Mass Spectrom.* **2002**, *220*, 399–418.
(22) Tyndall, A. M.; Powell, C. F. *Proc. R. Soc. A* **1930**, *129*, 162–180.
(23) Chen, C.; Chen, H.; Li, H. *Anal. Chem.* **2017**, *89*, 13398–13404.
(24) McGann, W. J.; Jenkins, A.; Ribiero, K.; Napoli, J. *SPIE Proceedings* **1993**, 64–75.
(25) Leonhardt, J. W.; Rohrbeck, W.; Bensch, H. *Int. J. Ion Mobil. Spec.* **2000**, 43–49.
(26) Chen, C.; Tabrizchi, M.; Wang, W.; Li, H. *Anal. Chem.* **2015**, *87*, 7925–7930.
(27) Zühlke, M.; Zenichowski, K.; Riebe, D.; Beitz, T.; Löhmannsröben, H.-G. *Int. J. Ion Mobil. Spec.* **2017**, *75*, 435 A.
(28) Zimmermann, S.; Kirk, A. T. *Method for operating an ion gate, device having an ion transport region*, 2. August 2016.
(29) Cochems, P.; Kirk, A. T.; Zimmermann, S. *Rev. Sci. Instrum.* **2014**, *85*, 124703.
(30) Verbeck, G. F.; Ruotolo, B. T.; Gillig, K. J.; Russell, D. H. *J Am Soc Mass Spectrom* **2004**, *15*, 1320–1324.
(31) Giles, K.; Grimsrud, E. P. *J. Phys. Chem.* **1992**, *96*, 6680–6687.
(32) Ewing, R. G.; Eiceman, G. A.; Harden, C. S.; Stone, J. A. *Int. J. Mass Spectrom.* **2006**, *255-256*, 76–85.
(33) Tabrizchi, M.; Khezri, E. *Int. J. Ion Mobil. Spec.* **2008**, *11*, 19–25.
(34) Kirk, A. T.; Raddatz, C.-R.; Zimmermann, S. *Anal. Chem.* **2017**, *89*, 1509–1515.
(35) Valentine, S. J.; Clemmer, D. E. *Anal. Chem.* **2009**, *81*, 5876–5880.

For TOC only